Predicting grain size in extruded AA6063 profiles: A unified approach based on finite element analysis and machine learning

Predicting Grain Size in Extruded AA6063 Profiles: A Unified Approach based on Finite Element Analysis and Machine Learning

Marco Negozio[1], Vincenzo Ferraro[1], Lorenzo Donati[2], Adrian H.A. Lutey[1]

[1]*Department of Engineering and Architecture – University of Parma*

Parco Area delle Scienze, 181/A, 43124 Parma, Italy.

[2]*DIN Department of Industrial Engineering – University of Bologna,*

Viale Risorgimento 2, 40136, Bologna, Italy.

CORRESPONDING AUTHOR:

Marco Negozio

Department of Engineering and Architecture – University of Parma

Parco Area delle Scienze, 181/A, 43124 Parma, Italy.

Tel. +39 052190 6029

e-mail: marco.negozio@unipr.it

Abstract

The evolution of grain size in AA6XXX extruded profiles is a critical factor for enhancing mechanical, thermal and surface properties. Traditional methods for microstructure control rely on extensive experiments requiring significant time and resources. To address this issue, the present work proposes a method for microstructure prediction combining numerical data from Finite Element Method (FEM) simulations with experimentally acquired microstructure data to train an Artificial Neural Network (ANN) capable of predicting grain size. Data was acquired for three distinct AA6063 aluminum alloy profiles extruded under various process conditions in terms of profile and tool geometry, ram speed, billet pre-heating temperature and extrusion ratio, representing a diverse and heterogenous dataset comprising grain size (55 – 228 μm), strain (2.8 – 28), maximum strain rate (2 – 190 s^{-1}), exit temperature (480 – 580 °C), Zener-Hollomon parameter (4×10^{15} – 4×10^{17}) and Stored Energy (170 – 480 kJ/mol*K) for training and testing different ANN configurations. The final trained ANN was able to accurately predict grain size in regions of normal grain growth but was less reliable at foreseeing formation of the largest and smallest grains due to limited data points within this range. A Mean Absolute Percentage Error (MAPE) of 13.9% was achieved for predictions in the test set with an ANN comprising two fully connected layers with 9 and 19 neurons, respectively, Rectified linear unit (ReLU) activation functions and a ridge L2 penalty term of 10^{-6} for regularization. The presented methodology provides a foundation for the development of new data-driven approaches aimed at facilitating microstructure prediction in industrial settings.

Keywords: Extrusion, Microstructure Prediction, Aluminum Alloy, Finite Element Method, Machine Learning, Artificial Neural Networks.

1. Introduction

AA6XXX extruded profiles employed in the automotive sector require a combination of mechanical and crash properties that can only be achieved through control of the microstructure [1]. Numerous material and process parameters influence grain evolution during extrusion, introducing a high level of complexity in controlling this aspect [2]. AA6063 aluminum alloy extruded profiles typically exhibit a statically recrystallized (SRX) structure, primarily due to the absence or near absence of dispersoids that would otherwise delay static recrystallization and favor a fibrous structure [3]. For this reason, it is essential to develop reliable SRX predictive models for industrial applications to facilitate die design and definition of optimal process parameters.

Significant effort has been devoted to the study of aluminum alloy extrusion through Finite Element Method (FEM) simulation. Various aspects of the process have been investigated, ranging from thermomechanical analysis [4][5] to process optimization [6][7]. FEM software has been used to simulate microstructural evolution occurring during the deformation process. Models have been developed for post-processing prediction of dynamically recrystallized grain sizes [8], statically recrystallized grain sizes [2][9] and prediction of surface recrystallization, also known as the Peripheral Coarse Grain (PCG) defect [10][11][12]. Within this context, the application of Machine Learning (ML) to extrusion may improve the capacity to recognize pertinent process relationships and identify correlations and causality that are not necessarily accounted for within analytical models, as well as the ability to represent a broader range of process conditions and materials.

ML has diverse applications across manufacturing for process optimization based on route cause analysis, prediction of manufacturing outcomes and diagnosis, allowing manual and automated corrective measures to be implemented with reduced expenditure, cycle time and scrap [13]. The main advantages of ML algorithms in manufacturing relate to their ability to handle high dimensional problems characterized by low transparency and discover previously unknown knowledge and relationships within data [14]. ML and ML-based optimization have been applied to milling [15][16], turning [17][18], gear hobbing [19], electrical discharge machining [20][21], injection molding [22] and welding [23][24], amongst others. In relation to metal forming, ML has been applied to the development of constitutive models [25] and prediction of deformation and flow stress behavior of specific metal alloys [26][27][28].

Artificial neural networks (ANNs) are of particular relevance to manufacturing processes due to their efficiency, performance and ease of implementation with standardized toolboxes. Inspired by biological neural networks, ANNs comprise a series of connected nodes, or neurons, that receive, process and emit signals to other connected neurons [29][30][31]. The structure and functionality of an ANN is governed by hyperparameters such as the number of fully connected layers, the number of neurons per layer, the type of activation function used to calculate neuron outputs from a given set of inputs and the learning rate employed to update network parameters during training [32][33]. Several works have seen ANNs applied to various aspects of extrusion, including prediction of the extrusion pressure [34][35], tensile strength distribution [36], deformation behavior [37] and exit temperature [38]. A combined approach employing FEM and ANN has been developed for prediction of the extrusion load of AA1070 aluminum alloy, reducing requirements for lengthy experimental analyses [39]. ANNs have also been used to predict die failure during hot extrusion of AA6063 aluminum alloy [40], as well as to assist in die design for flow balance [41]. To the authors' best knowledge, ANNs have not yet been applied to the prediction of grain size in extruded profiles.

To explore the potential benefits and limitations of ML applied to predicting microstructural outcomes during extrusion, the present work combines FEM with ANNs to predict grain size

evolution in AA6063 extruded profiles. The approach combines FEM simulations with experimental microstructure data to train an ANN representation of the extrusion process capable of predicting the resulting grain size based on FEM simulation outputs. To implement the proposed approach, grain size data was acquired from three different AA6063 alloy profiles, with FEM simulations developed in each case to extract numerical data relevant to microstructural evolution. Training and testing of neural networks was then performed to develop a data-driven model of grain size based on FEM simulation outputs. With optimized hyperparameters, prediction accuracy of the trained neural network was found to be in line with analytical approaches [2][3], providing a foundation for developing reliable and automated data-drive models with greater versatility and ease of implementation in industrial settings.

2. Materials and Methods

2.1 General approach

The developed methodology, depicted schematically in Fig. 1, comprised acquiring experimental and FEM simulation data pertaining to the extrusion of three different AA6063 alloy profiles obtained with different process parameters. FEM simulations were performed with Qform Extrusion UK [42][43] to calculate relevant numerical parameters potentially influencing microstructural evolution within various regions. Known recrystallization model parameters were then calculated based on FEM outcomes. The grain size of AA6063 alloy extruded profiles was determined experimentally within the same regions via metallographic analysis. All data were then randomly assigned to training and test sets with a division of 80/20%. The former was utilized to train a feed-forward, fully connected ANN for regression within MATLAB using the *fitrnet* function [45], considering data deriving from FEM simulations as inputs and the resulting grain size within the same regions as outputs. Model performance was then assessed by comparing the predicted and true grain sizes within the test set.

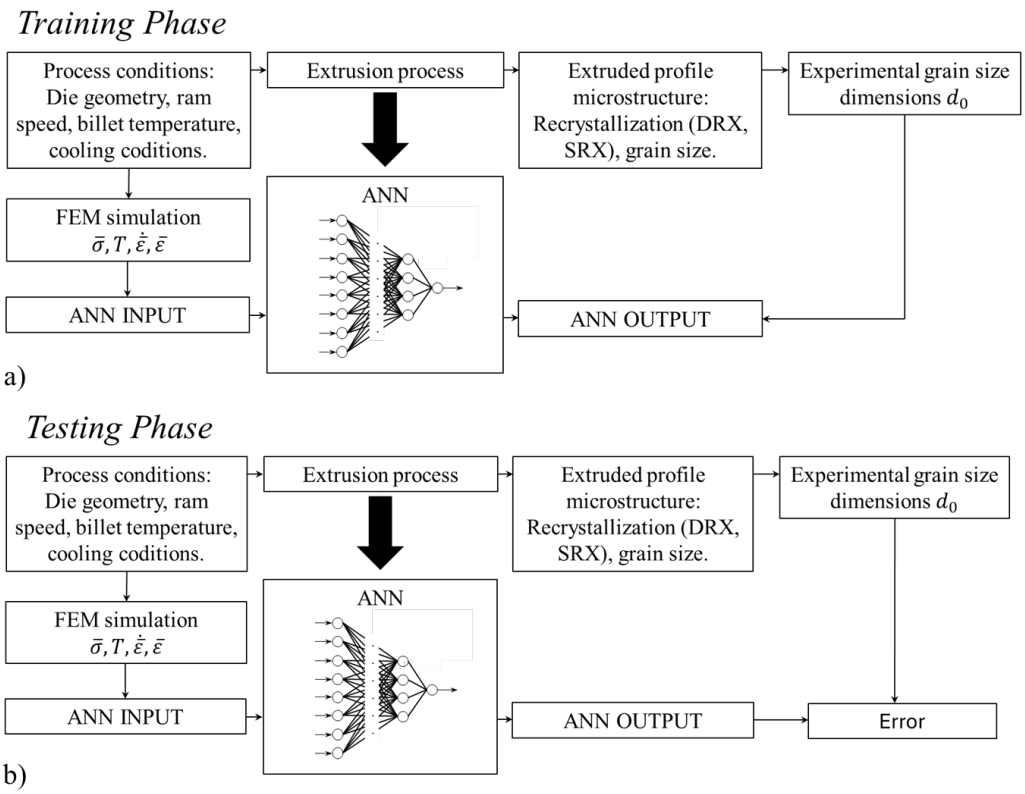

Figure 1: Schematic of the combined FEM-ML approach: a) training and b) testing phases.

2.2 Experimental Investigation

Three dies with geometries as reported in Fig. 2 were employed for extrusion of AA6063 aluminum alloy profiles. Profile 1 was extruded by Indinvest LT Srl in Latina, Italy, Profile 2 by Hydro Extrusion Italy Srl in Ornago, Italy, and Profile 3 by Hydro Extruded Solutions AB in Finspang, Sweden. The dies were manufactured by Almax Mori Srl (Profile 1), Phoenix International SpA (Profile 2) and Hydro Extruded Solutions AB (Profile 3), respectively. As can be observed in Fig. 2, the profiles exhibited entirely different geometries, thus providing diverse and heterogeneous data to enhance the relevance of training and testing data employed to assess the developed methodology. Profile 1 featured two exits, each comprising a solid profile with a thick central part surrounded by two small ribs. Profile 2 was a hollow profile designed with much larger dimensions than the other two. Profile 3 was instead a compact profile comprising a central round bar and two lateral ribs.

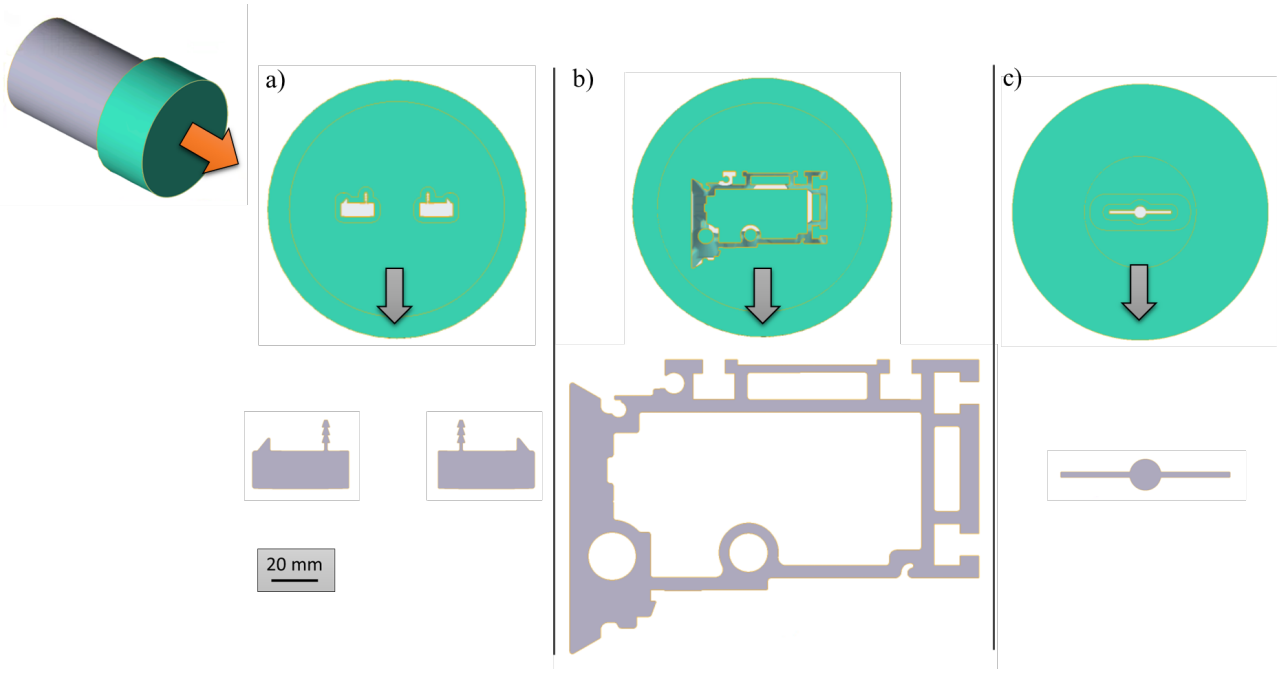

Figure 2: AA6063 profiles employed for experiments: a) Profile 1, b) Profile 2 and c) Profile 3.

Process conditions employed for extrusion of all profiles are shown in Table 1. As noted previously, an extensive range of conditions was considered to provide diverse and heterogeneous data for assessment of the employed approach. Profile 1 and Profile 3 exhibited the highest extrusion ratios, 44 and 46 respectively, while Profile 2 was characterized by a relatively low ratio of 9.6. The ram speed was 6.4 mm/s for Profile 1, 8.5 mm/s for Profile 2 and 9.1 mm/s for Profile 3, while the preheating temperatures were 530°C, 470°C and 490°C, respectively. Table 1 also provides information relating to differences in geometry, including the lengths of the respective billets, 670 mm for Profile 1, 815 mm for Profile 2, and 270 mm for Profile 3, as well as the dimensions of the overall components involved. Profiles 1 and 2 were extruded using industrial presses, whereas Profile 3 was extruded using a laboratory press.

Table 1: Extrusion process parameters.

Process parameters and tool/workpiece geometries	Profile 1	Profile 2	Profile 3
Extrusion press capacity [MN]	35	30	10
Extrusion ratio	44	9.6	46
Ram speed [mm/s]	6.4	8.5	9.2
Ram acceleration time [s]	5	5	5
Billet temperature [°C]	530	470	490
Die temperature [°C]	450	450	400
Container temperature [°C]	430	420	400
Billet length [mm]	670	815	270
Billet diameter [mm]	254	247	100
Container diameter [mm]	264	257	107
Billet Rest length [mm]	15	55	15

Experimental grain size data were acquired following standard metallographic procedures. Extruded profiles were sectioned, ground, polished and electrochemically etched with anodization performed

at 40 V DC for 4 minutes. Samples were then observed using a polarized light optical microscope, highlighting differences in grain orientations. Grain sizes were then determined according to ASTM E112-13 at random locations on profile sections to obtain a dataset that comprehensively described the microstructure of all profiles. Once collected, these data were considered output values for training and testing of the ANN.

2.3 Finite Element Simulation

Simulations of the extrusion processes employed to obtain the three profiles were conducted in line with the specific conditions applied in each case to obtain numerical values as inputs for training and testing of the ANN. The commercial software package QForm Extrusion UK [42][43] was employed, representing an optimized tool for studying the extrusion process using an Arbitrary Lagrangian Eulerian (ALE) approach. Simulations were conducted in line with a method described in a previous work [3], where simulation and convergence parameters were optimized to simulate the extrusion process of aluminum alloys. Sticking friction was considered at the interface surfaces between the billet and die/ram/container, while the Levanov friction model (m = 0.3, n = 1.25) was applied to account for friction between the workpiece and bearing zone. In relation to numerical parameters, Qform Extrusion UK generates and optimizes tool and workpiece meshes with adjustable mesh parameters for greater precision. While standard values are recommended for efficiency, the simulations performed in the present work were generated with the highest settings, thus employing the finest possible mesh. Although this resulted in longer simulation times, these remained consistently below two hours, acceptable within an industrial simulation context [2]. Tetrahedral 4-node elements were employed in all cases, with 87359, 208410 and 29728 elements employed for representation of the tool and 76846, 267895 and 17141 elements employed for representation of the workpiece for Profiles 1, 2 and 3, respectively.

The Hensel-Spittel law was chosen to calculate flow stress (Eq. 1), employing the optimized parameters reported in [3] for AA6063, shown in Tab. 2. This representation was chosen as it is one of the most complete models developed to date, employing nine parameters that can be determined experimentally, enabling complete characterization of materials such as aluminum alloys. According to this law, the flow stress of a given material is defined as a function of the strain, strain rate and temperature, all of which are calculated directly by software using FEM.

$$\bar{\sigma} = A \cdot e^{m_1 T} \cdot \bar{\varepsilon}^{-m_2} \cdot \dot{\bar{\varepsilon}}^{-m_3} \cdot e^{\frac{m_4}{\bar{\varepsilon}}} \cdot (1+\bar{\varepsilon})^{m_5 T} \cdot e^{m_7 \bar{\varepsilon}} \cdot \dot{\bar{\varepsilon}}^{m_8 T} \cdot T^{m_9} \quad (1)$$

Table 2: Hensel-Spittel flow stress law and parameters adopted for AA6063 [3].

Coefficients	AA6063
A [MPa]	1014.7
m1[K^{-1}]	-0.00438
m2	0.2425
m3	-0.0965
m4	-0.000438
m5 [K^{-1}]	-0.000766
m7	0.002939
m8 [K^{-1}]	0.000291
m9	0

Before collecting numerical values for the training and testing datasets, experimentally measured exit temperatures and extrusion load values were compared with simulated values to assess the accuracy of the FEM simulation. The results of this comparison are shown in Table 3. The error was consistently below 2% in most cases and 5% in all cases.

Table 3: Comparison between experimental and numerical profile exit temperatures and peak extrusion loads.

	Profile *1*	Profile *2*	Profile *3*
Experimental profile exit temperature [°C]	557 ±5	542 ±5	433 ±5
Simulated profile exit temperature [°C]	562	539	438
Error [%]	<1	<1	1.1
Experimental peak extrusion load [MN]	23.4 ±0.1	26.00 ±0.1	3.47 ±0.10
Simulated peak extrusion load [MN]	23.3	26.51	3.31
Error [%]	<1	1.9	4.6

2.4 Artificial Neural Network (ANN)

An ANN representation of microstructural evolution was developed with MATLAB using the *fitrnet* function [45]. The dataset of approximately 350 samples was randomly assigned to training and test sets with a division of 80/20%. Available input variables were those deriving from the FEM simulation, while the output was the microstructure grain size. The former included standard outputs from the FEM simulation including temperature, stress, strain and strain rate, as well as addition data deriving from simulations. The maximum strain rate was calculated and stored automatically within QForm Extrusion UK via a customized subroutine that computed the evolution of strain-rate values for each point along the deformation path from the billet to the exit profile, retaining only the highest value in each position [10]. The Zener-Hollomon parameter and the Stored Energy value were also considered as input variables, calculated according to the Negozio-Donati recrystallization model [3] as follows:

$$\frac{1}{\delta} = C\ (lnZ)^n \tag{2}$$

$$Z = \ \dot{\varepsilon}\ exp\ \left(\frac{Q}{RT}\right) \tag{3}$$

$$\mathrm{Pd} = \frac{Gb^2}{10}\left[\rho_i(1\text{-}\ln(10b\rho_i^{0,5}))+\frac{2\theta}{b\delta} * \left(1 + \ln\left(\frac{\theta c}{\theta}\right)\right)\right] \tag{4}$$

where Z is the Zener-Hollomon parameter, T the exit temperature, Pd the Stored Energy, C = 3.36×10^{-9} m^{-1}, n = 5.577, Q the activation energy of AA6063 (232350 J/mol*K [3]), $\dot{\varepsilon}$ the maximum strain rate, R the universal gas constant (8.341 J/mol), G the material shear modulus (2.05×10^{10} Pa [3]), b the Burgers vector (2.86×10^{-10} m [3]), ρ_i the dislocation density, δ the subgrain size, Θ the misorientation angle and Θc the misorientation angle limit (15°) [10]. The Negozio-Donati SRX model was selected due to its proven accuracy in predicting the grain size of fully statically recrystallized AA6063 alloy structures in a previous study [3].

Input variables for the ANN model were chosen to be as independent as possible, with correlated variables limited to those bound by non-linear functions; specifically, Z and Pd. To determine the final set of input variables, experiments were performed by training and testing various ANN configurations to determine the sensitivity of model outcomes to each variable. Based on this investigation, greatest accuracy was achieved for a given ANN configuration by considering the exit temperature, plastic strain, maximum strain rate, maximum Zener-Holloman and Stored Energy as the input parameters. The full dataset employed for training and testing the ANN is provided in Table 5 in the Appendix.

ANN hyperparameter optimization was performed by identifying reasonable parameter ranges over which the model could be expected to provide accurate outcomes while avoiding excessive model complexity or overfitting. In particular, the number of fully connected layers and number of neurons per layer were limited due to the relatively low number of input variables and available data. Grid optimization was performed over the parameter ranges shown in Table 4. Standardization was employed in all cases due to large variations in the scale of input parameters. The set of hyperparameters leading to the lowest Mean Absolute Percentage Error (MAPE) are provided in the righthand column of Table 4. Detailed evaluation of the outcomes of hyperparameter optimization is provided in the following section.

Table 4: ANN hyperparameter ranges tested during optimization and chosen values.

	Tested range	Chosen values
Activation function for fully connected layers	Rectified linear unit (ReLU); Hyperbolic tangent (tanh); Sigmoid	Rectified linear unit (ReLU)
Number of fully connected layers	1 – 2	2
Number of neurons per layer	1 – 50	Layer 1: 9 Layer 2: 19
Regularization term strength (ridge L2 penalty term)	10^{-8} – 100	10^{-6}

3. Results and Discussion

3.1 Experimental Investigation

Figure 3 presents complete microstructures of sections obtained from all three experimentally extruded profiles, as well as an example of detailed micrographs obtained for Profile 2 within specific regions indicated in Fig. 3a. All of the analyzed profiles were characterized by static recrystallization after deformation during the hot extrusion process, as AA6063 alloy exhibits few or no dispersoids and therefore low resistance to recrystallization [3]. As a result, the experimentally determined grain size ranged from 60 µm to 140 µm for Profile 1, from 55 µm to 228 µm for Profile 2 and from 55 µm to 120 µm for Profile 3. The relative frequency of grain sizes within the complete dataset are provided in Fig. 4, where it can be observed that the majority of measurements fell within the range 75 – 140 µm, which is the typical grain size in AA6063 extruded profiles [46], with a limited number of values outside this range down to 55 µm and up to 228 µm.

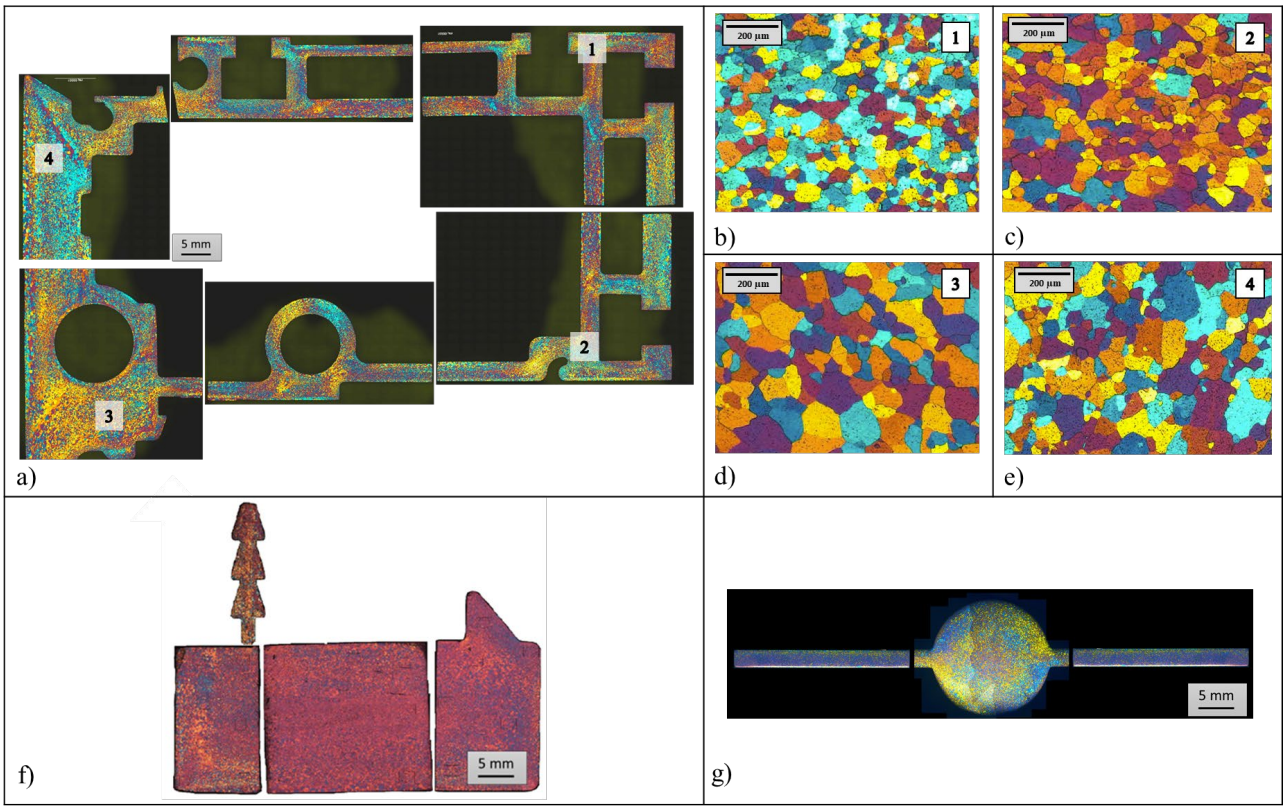

Figure 3: Experimentally determined microstructures of: a) Profile 2, b-e) Profile 2 within specific regions f) Profile 1, and g) Profile 3.

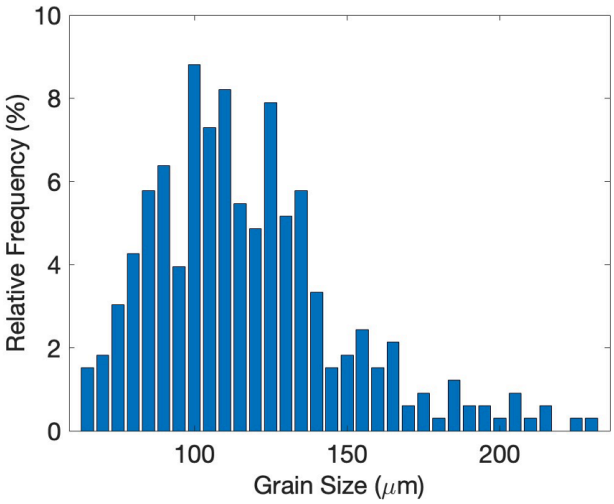

Figure 4: Relative frequency of experimental grain size measurements within entire dataset.

3.2 Finite Element Simulation

The strain, maximum strain rate, temperature, Zener-Hollomon and Stored Energy were calculated from FEM simulation data within the same regions in which the experimental grain size was determined. Strain and temperature values were derived directly from standard outputs of the FEM simulation, while the maximum strain rate, Zener-Hollomon parameter and Stored Energy were calculated via a customized subroutine. As an example of the obtained output, Fig. 5 displays the strain, maximum strain rate and temperature distributions for Profile 2, where it can be seen that the plastic strain and maximum strain rate attained highest values at the surface and in longitudinal welding zones. Instead, the temperature attained highest values at the inner surface and minimum

values on the righthand side of the profile, as depicted in Fig. 5d. Figure 6 instead displays the relative frequencies of all variables within the entire dataset. Values of strain and maximum strain rate were generally concentrated within the ranges 4 – 8 and 5 – 25 s^{-1}, respectively, with more limited instances of higher values. The temperature distribution was centered around 540 °C, with decreasing frequency down to 460 °C and up to 580 °C. The Zener-Hollomon parameter exhibited highest frequency at 2 × 10^{16}, with all values in the range 4×10^{15} – 4×10^{17}, while the Stored Energy was centered around 240 × 10^{5} kJ/mol*K with all values in the range 170 – 480 kJ/mol*K. The range of input variables employed for training the ANN was therefore broad and representative of conditions commonly encountered in the majority of industrial extrusion processes [2][3][46]. The limited frequency of very high and very low values of some parameters was no doubt a limiting factor; however, collection of additional data within these regions would have required extrusion to be performed outside of typical operating conditions, leading to additional complexities beyond the scope of the present investigation.

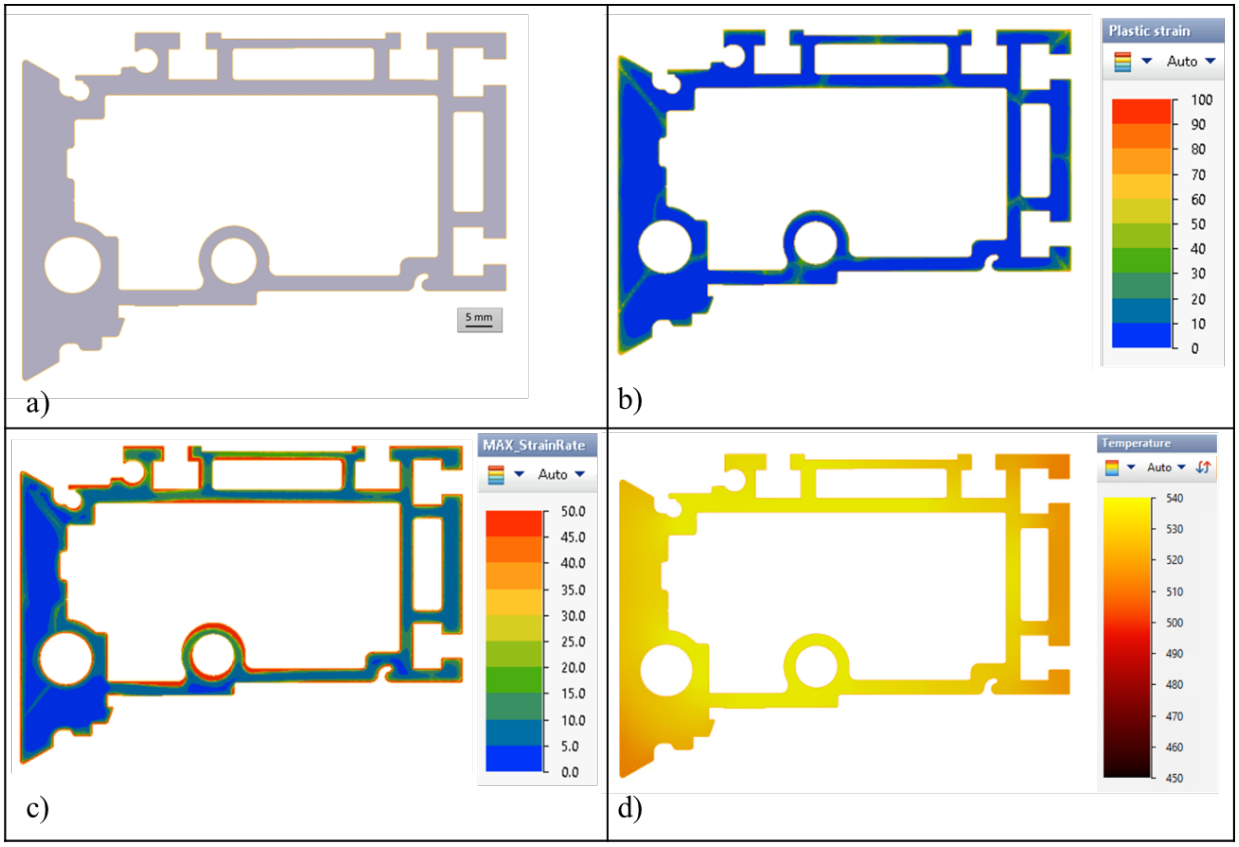

Figure 5: FEM simulation outputs for Profile 2: a) geometry, b) strain, c) maximum strain rate and d) temperature.

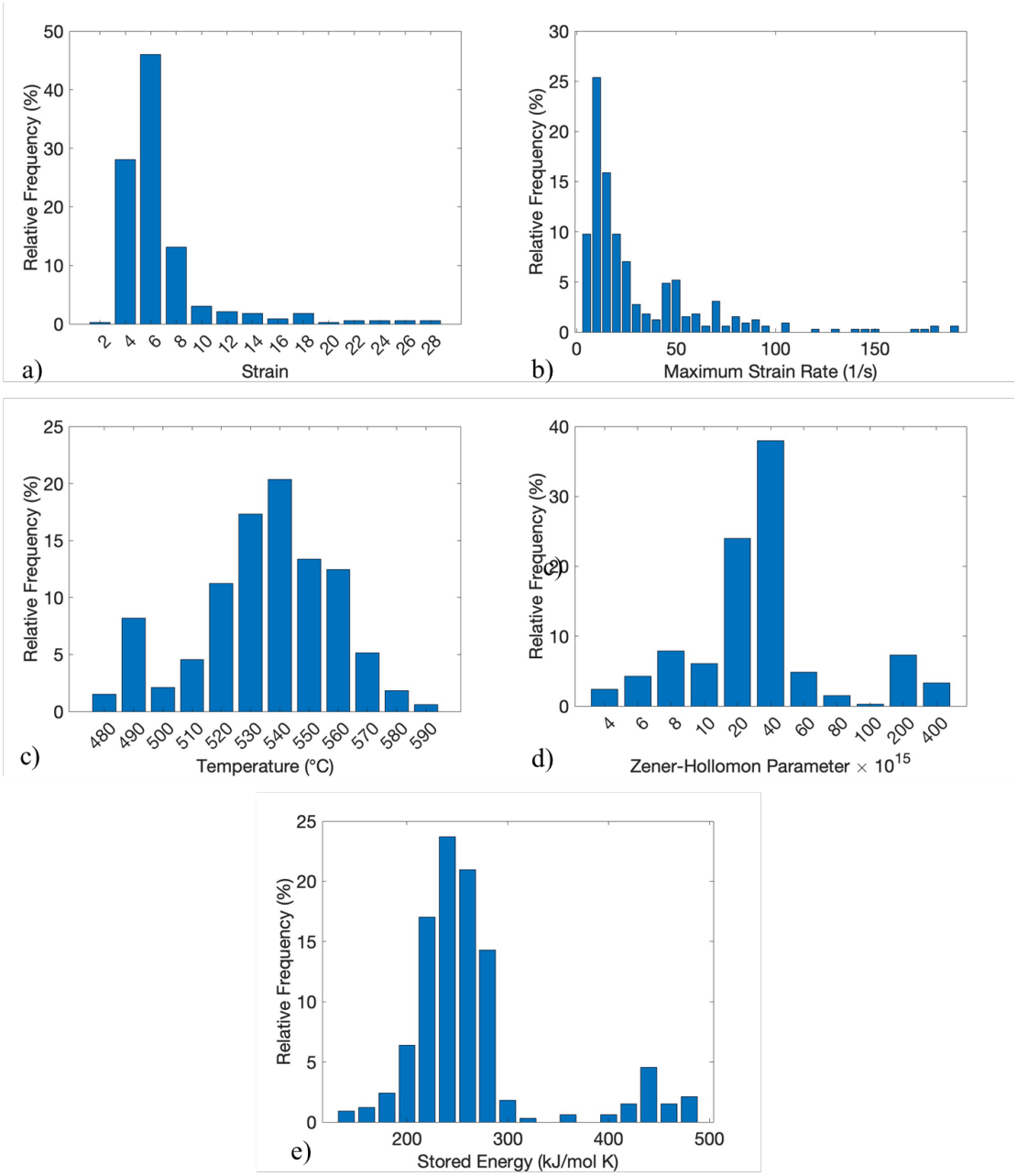

Figure 6: Relative frequency of simulated a) strain, b) maximum strain rate, c) exit temperature, d) Zener-Hollomon parameter and e) store energy within entire dataset.

3.3 Neural Network

The outcomes of hyperparameter optimization performed with the training dataset are shown graphically in Fig. 7, where the MAPE is displayed as a function of the number of neurons in the first and second fully connected layers, activation function and regularization term strength (ridge L2 penalty term) while holding all other parameters constant at their optimum values. The obtained value of MAPE was found to be moderately sensitive to the activation function (optimal: ReLU) and regularization strength (optimal: 10^{-6}). A relatively complex relationship was instead observed for the number of neurons per layer, with fluctuations observed due to the limited number of available data. It was nonetheless observed that error was strongly dependent on the number of neurons in the first fully connected layer but less so for the second fully connected layer. An initial increase in neurons in the first fully connected layer led to a reduction in MAPE, after which a clear increasing trend was observed with increasing neurons at high values (optimal: 9 neurons). While less evident, the obtained

value of MAPE was also found to decrease with increasing neurons in the second layer for low values, before increasing once again (optimal: 19 neurons). The lowest value of MAPE achieved was 13.9%. With a single fully connected layer, the lowest value of MAPE achieved was 14.7% with 10 neurons. A minor but notable improvement was therefore obtained with the addition of a second fully connected layer. Hyperparameter optimization was clearly influenced by the limited size of the training dataset, suggesting that, while trends could be adequately observed in the present case, larger volumes of data would contribute to improving model accuracy. A schematic of the final ANN structure with the hyperparameters listed in the right-hand column of Tab. 4 is provided in Fig. 8.

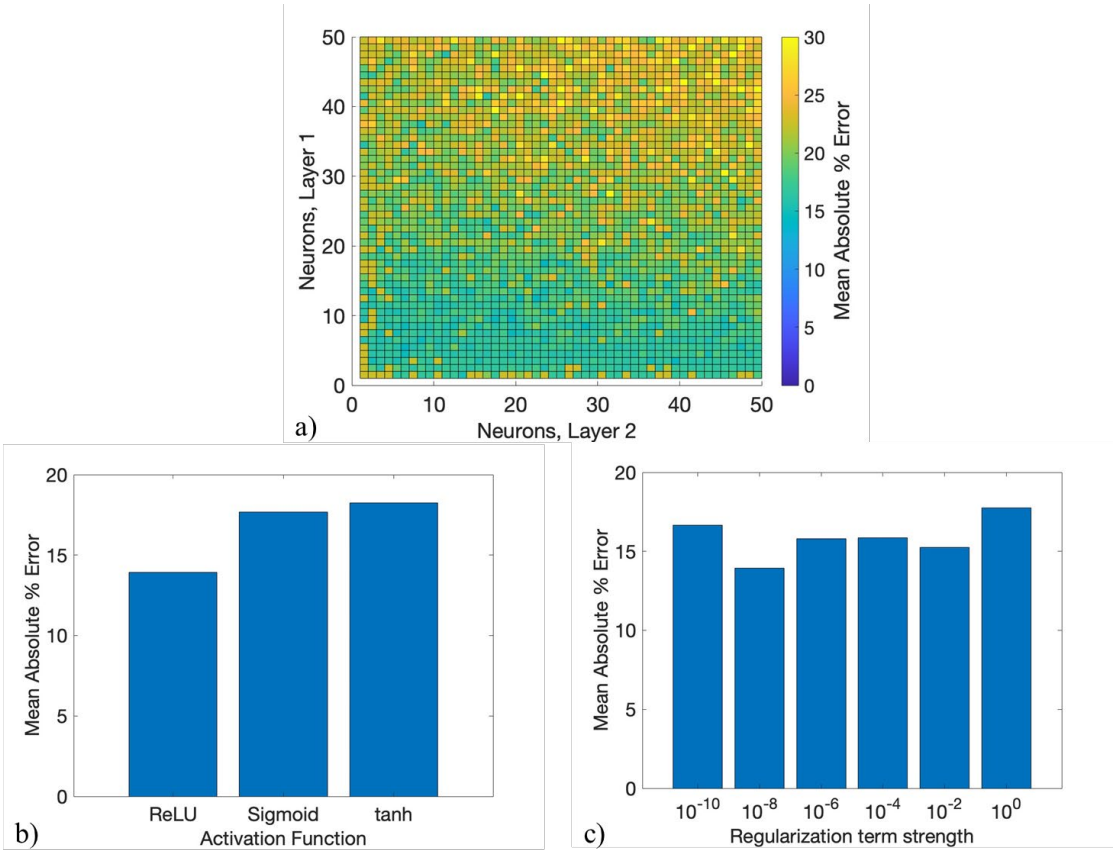

Figure 7: ANN hyperparameter optimization: mean absolute percentage error (MAPE) a) as a function of the number of neurons (ReLU activation function, 10^{-6} regularization term strength), b) as a function of the activation function (Layer 1: 9 neurons, layer 2: 19 neurons, 10^{-6} regularization term strength) and c) as a function of the regularization term strength (Layer 1: 9 neurons, layer 2: 19 neurons, ReLU activation function).

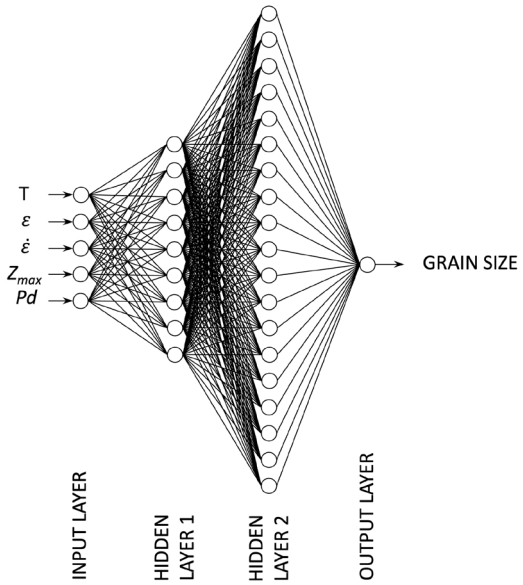

Figure 8: Schematic of final ANN with optimized hyperparameters.

Fig. 9 presents a comparison of the predicted and experimental grain size within the test set based on the trained ANN with optimized hyperparameters. The red line represents exact correspondence between the predicted and true values, while the dashed blue lines represent error limits of +/- 25%. This range was chosen as a suitable interval indicating good correspondence between the predicted and true grain size based on the outcomes of previous studies, noting that the measurement system itself entails approximations due to the choice of section and methodology for quantifying grain size [2][3][46]. The majority of data (>81%) fell within an absolute percentage error of less than 25%, while the mean error was 13.9%, confirming reasonable accuracy of the prediction via the trained ANN in the majority of cases. Larger percentage deviations were observed for the largest and smallest grain sizes due to the limited number of data points within these ranges in the original dataset (Fig 4). The relative frequency of the percentage error is presented in Fig. 10, where it can again be observed that the majority of data fell within the range +/-25%.

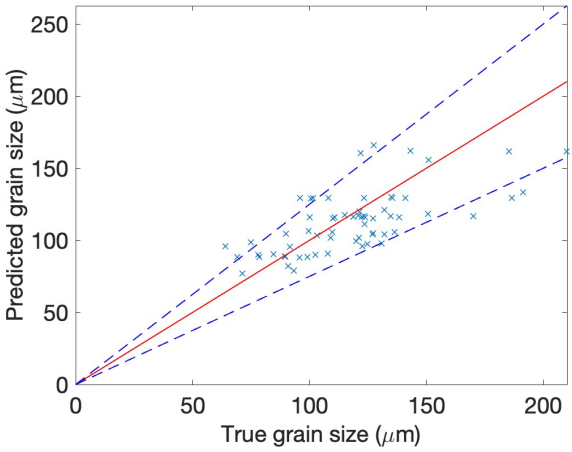

Figure 9: Predicted vs. true grain size, test dataset with trained ANN.

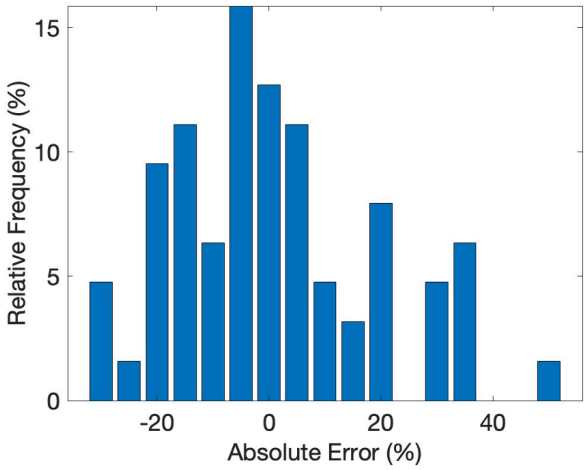

Figure 10: Relative frequency of predicted grain size absolute error, test dataset with trained ANN.

4. Conclusion

By combining Finite Element Method (FEM) simulations with an Artificial Neural Network (ANN), it was possible to predict the grain size of AA6063 hot extruded profiles with a Mean Absolute Percentage Error (MAPE) of 13.9% and more than 81% of predictions within the range of +/-25% error. In terms of prediction accuracy, these outcomes are in line with analytical methods, noting the inherent uncertainty in determining grain size experimentally. The main limiting factor of the present study was the quantity of available data, which, in light of the results, was adequate but not optimal. Further research is therefore undoubtedly required to collect additional data over a diverse range of conditions to improve ANN performance.

A significant result of this work lies in its proposed methodology. The insights gained from this approach will be harnessed to extend the predictive capabilities of the trained neural network to other areas, including combined models capable of dealing with variations in materials and process conditions. These include forecasting occurrence of the Peripheral Coarse Grain (PCG) defect, as well as understanding the influence of various parameters, both geometric (die design) and process-related, on the mechanical, crash and aesthetic properties of extruded profiles. Consequently, the accuracy of the predictions observed in this study marks a pivotal achievement for the development of subsequent predictive models based on data-driven models manufacturing.

DECLARATIONS:

Acknowledgements: not applicable

Funding: not applicable

Conflicts of interest/Competing interests: Authors do not have a financial relationship with the organization that sponsored the research. They should also have full control of all primary data and agree to allow the journal to review their data, if requested.

Availability of data and material: not applicable

Code availability: commercial code Qform UK (software application), MATLAB

References

[1] Sheppard T. Prediction of structure during shaped extrusion and subsequent static recrystallisation during the solution soaking operation. Journal of Materials Processing Technology 177, 26–35 (2006). https://doi.org/10.1016/j.jmatprotec.2006.04.099.
[2] Donati L., Segatori A., El Mehtedi M., Tomesani L. Grain evolution analysis and experimental validation in the extrusion of 6XXX alloys by use of a lagrangian FE code. International Journal of Plasticity 46, 70-81 (2013). https://doi.org/10.1016/j.ijplas.2012.11.008.
[3] Negozio M., Pelaccia R., Donati L., Reggiani B. Simulation of the microstructure evolution during the extrusion of two industrial-scale AA6063 profiles. Journal of Manufacturing Processes 99, 501-512 (2023). https://doi.org/10.1016/j.jmapro.2023.05.075.
[4] Yi J., Wang Z.H., Liu Z.W., Zhang J.M., He X. Fe analysis of extrusion defect and optimization of metal flow in porthole die for complex hollow aluminium profile. Transactions of Nonferrous Metals Society of China 28(10), 2094-2101 (2018). https://doi.org/10.1016/S1003-6326(18)64853-8.
[5] Zhang, C., Yang, S., Wang, C. et al. Numerical and experimental investigation on thermo-mechanical behavior during transient extrusion process of high-strength 7XXX aluminum alloy profile. Int J Adv Manuf Technol 85, 1915–1926 (2016). https://doi.org/10.1007/s00170-016-8595-3.
[6] Negozio, M., Pelaccia, R. Numerical, experimental, and analytical investigation of the skin contamination evolution in the extrusion of different industrial profiles. Int J Adv Manuf Technol (2024). https://doi.org/10.1007/s00170-024-13329-w.
[7] Giarmas, E., Tzetzis, D. Optimization of die design for extrusion of 6xxx series aluminum alloys through finite element analysis: a critical review. Int J Adv Manuf Technol 119, 5529–5551 (2022). https://doi.org/10.1007/s00170-022-08694-3.
[8] Güzel, A. Jäger A., F. Parvizian F. et al. A new method for determining dynamic grain structure evolution during hot aluminum extrusion. Journal of Materials Processing Technology 212(1), 323-330 (2012). https://doi.org/10.1016/j.jmatprotec.2011.09.018.
[9] Schikorra, M., Donati, L., Tomesani, L. et al. Microstructure analysis of aluminum extrusion: grain size distribution in AA6060, AA6082 and AA7075 alloys. J Mech Sci Technol 21, 1445–1451 (2007). https://doi.org/10.1007/BF03177357.
[10] Negozio, M., Pelaccia, R., Donati, L. et al. Numerical investigation of the surface recrystallization during the extrusion of a AA6082 aluminum alloy under different process conditions. Int J Adv Manuf Technol 129, 1585–1599 (2023). https://doi.org/10.1007/s00170-023-12397-8.
[11] Negozio M., Segatori A., Pelaccia R., Reggiani B., Donati L. Experimental investigation and numerical prediction of the peripheral coarse grain (PCG) evolution during the extrusion of different AA6082 aluminum alloy profiles. Materials Characterization 209, 113723 (2024). https://doi.org/10.1016/j.matchar.2024.113723.
[12] Mahmoodkhani, Y., Chen, J., Wells, M.A. et al. The Effect of Die Bearing Geometry on Surface Recrystallization During Extrusion of an Al-Mg-Si-Mn Alloy. Metall Mater Trans A 50, 5324–5335 (2019). https://doi.org/10.1007/s11661-019-05437-0.
[13] Weichert, D., Link, P., Stoll, A. et al. A review of machine learning for the optimization of production processes. Int J Adv Manuf Technol 104, 1889–1902 (2019). https://doi.org/10.1007/s00170-019-03988-5.
[14] Wuest T., Weimer D., Irgens C., Thoben K.D. Machine learning in manufacturing: advantages, challenges, and applications. Production & Manufacturing Research 4(1), 23-45 (2016). https://doi.org/10.1080/21693277.2016.1192517.
[15] Coppel R., Abellan-Nebot J.V., Siller H.R. et al. Adaptive control optimization in micro-milling of hardened steels—evaluation of optimization approaches. Int J Adv Manuf Technol 84, 2219–2238 (2016). https://doi.org/10.1007/s00170-015-7807-6.
[16] Kant G., Sangwan K.S. Predictive Modelling and Optimization of Machining Parameters to Minimize Surface Roughness using Artificial Neural Network Coupled with genetic algorithm. Procedia CIRP 31, 452-458 (2015). https://doi.org/10.1016/j.procir.2015.03.043.
[17] Gupta A.K., Guntuku S.C., Desu R.K. et al. Optimisation of turning parameters by integrating genetic algorithm with support vector regression and artificial neural networks. Int J Adv Manuf Technol 77, 331–339 (2015). https://doi.org/10.1007/s00170-014-6282-9.
[18] Bouacha K., Terrab A. Hard turning behavior improvement using NSGA-II and PSO-NN hybrid model. Int J Adv Manuf Technol 86, 3527–3546 (2016). https://doi.org/10.1007/s00170-016-8479-6.
[19] Cao W.D., Yan C.P., Ding L. et al. A continuous optimization decision making of process parameters in high-speed gear hobbing using IBPNN/DE algorithm. Int J Adv Manuf Technol 85, 2657–2667 (2016). https://doi.org/10.1007/s00170-015-8114-y.
[20] Assarzadeh S., Ghoreishi M. Neural-network-based modeling and optimization of the electro-discharge machining process. Int J Adv Manuf Technol 39, 488–500 (2008). https://doi.org/10.1007/s00170-007-1235-1.

[21] Majumder A. Comparative study of three evolutionary algorithms coupled with neural network model for optimization of electric discharge machining process parameters. Proceedings of the Institution of Mechanical Engineers, Part B: Journal of Engineering Manufacture 229(9), 1504-1516 (2015). https://doi.org/10.1177/0954405414538960.
[22] Xu G., Yang Z. Multiobjective optimization of process parameters for plastic injection molding via soft computing and grey correlation analysis. Int J Adv Manuf Technol 78, 525–536 (2015). https://doi.org/10.1007/s00170-014-6643-4.
[23] Norouzi A., Hamedi M., Adineh, V.R. Strength modeling and optimizing ultrasonic welded parts of ABS-PMMA using artificial intelligence methods. Int J Adv Manuf Technol 61, 135–147 (2012). https://doi.org/10.1007/s00170-011-3699-2.
[24] Rong Y., Zhang G., Chang Y. et al. Integrated optimization model of laser brazing by extreme learning machine and genetic algorithm. Int J Adv Manuf Technol 87, 2943–2950 (2016). https://doi.org/10.1007/s00170-016-8649-6.
[25] Lourenço R., Andrade-Campos A., Georgieva P. The Use of Machine-Learning Techniques in Material Constitutive Modelling for Metal Forming Processes. Metals 12, 427 (2022). https://doi.org/10.3390/met12030427.
[26] Toros S., Ozturk F. Flow curve prediction of Al–Mg alloys under warm forming conditions at various strain rates by ANN. Applied Soft Computing 11(2) 1891-1898 (2011). https://doi.org/10.1016/j.asoc.2010.06.004.
[27] Mandal S., Sivaprasad P.V., Venugopal S., Murthy K.P.N. Artificial neural network modeling to evaluate and predict the deformation behavior of stainless steel type AISI 304L during hot torsion. Applied Soft Computing 9(1) 237-244 (2009). https://doi.org/10.1016/j.asoc.2008.03.016.
[28] Sheikh H., Serajzadeh S. Estimation of flow stress behavior of AA5083 using artificial neural networks with regard to dynamic strain ageing effect, Journal of Materials Processing Technology 196(1-3), 115-119 (2008). https://doi.org/10.1016/j.jmatprotec.2007.05.027.
[29] Bishop C.M. Neural networks and their applications, Review of Scientific Instruments 65(6), 1803-1832 (1994). https://doi.org/10.1063/1.1144830.
[30] Gurney K. An Introduction to Neural Networks, 1st Edition, CRC Press, 1997. https://doi.org/10.1201/9781315273570.
[31] Haykin S.S. Neural Networks and Learning Machines, Volume 10, Prentice Hall, 2009, ISBN 9780131471399.
[32] Samarasinghe S. Neural Networks for Applied Sciences and Engineering, 1st Edition, Auerbach Publications, 2006. https://doi.org/10.1201/9780849333750.
[33] Alanis A.Y., Arana-Daniel N., López-Franco C. (eds.) Artificial Neural Networks for Engineering Applications, Elsevier Inc., 2019, ISBN 9780128182475.
[34] Li Y.Y., Bridgwater J. Prediction of extrusion pressure using an artificial neural network, Powder Technology 108(1) 65-73 (2000). https://doi.org/10.1016/S0032-5910(99)00254-5.
[35] Abdul Jawwad A.K., Barghash M.A. Evaluating the effects of process parameters on maximum extrusion pressure using a new artificial neural network-based (ANN-based) partial-modeling technique. Int J Adv Manuf Technol 68, 2547–2564 (2013). https://doi.org/10.1007/s00170-013-4852-x.
[36] Hsiang SH., Kuo JL., Yang, FY. Using Artificial Neural Networks to Investigate the Influence of Temperature on Hot Extrusion of AZ61 Magnesium Alloy. J Intell Manuf 17, 191–201 (2006). https://doi.org/10.1007/s10845-005-6636-0.
[37] Qin Y.J., Pan Q.L., He Y.B., Li W.B., Liu X.Y., Fan X. Artificial Neural Network Modeling to Evaluate and Predict the Deformation Behavior of ZK60 Magnesium Alloy During Hot Compression, Materials and Manufacturing Processes 25(7), 539-545 (2010). https://doi.org/10.1080/10426910903124894.
[38] Zhou J., Li L. X., Mo J., Zhou J., Duczczyk, J. Prediction of the Extrusion Load and Exit Temperature Using Artificial Neural Networks Based on FEM Simulation. Key Engineering Materials 424, 241–248 (2009). https://doi.org/10.4028/www.scientific.net/kem.424.241.
[39] Bingöl S., Ayer Ö., Altinbalik, T. Extrusion load prediction of gear-like profile for different die geometries using ANN and FEM with experimental verification. Int J Adv Manuf Technol 76, 983–992 (2015). https://doi.org/10.1007/s00170-014-6328-z.
[40] Almutahhar M., Alhajeri A., Laghari R.A. et al. Prediction of tool failure in metal hot extrusion process using artificial neural networks. Materials Research Proceedings 36, 8-15 (2023). https://doi.org/10.21741/9781644902790-2.
[41] Yu Y.B., Lai Y.R., Hsu Q.C., Truong T.T. Deep Convolutional Neural Network to Assist Die Design for Flow Balance of Aluminum Hollow Extrusion. Lecture Notes in Mechanical Engineering (2024). https://doi.org/10.1007/978-3-031-42093-1_7.

[42] Stebunov S., Lishnij A., Biba N. Development and industrial verification of QForm-Extrusion program for simulation profile extrusion in: Proceeding of International Conference on Extrusion and Benchmark, Dortmund, Germany, 41-42 (2009).
[43] Kniazkin I., Pelaccia R., Negozio M., Di Donato S., Donati L., Reggiani B., Biba N., Rezvykh R., Kulakov I. Investigation of the skin contamination predictability by means of QForm UK extrusion code, Materials Research Proceedings 28, 543-552 (2023). https://doi.org/10.21741/9781644902479-59.
[44] Negozio, M., Pelaccia, R., Donati, L. et al. Numerical investigation of the surface recrystallization during the extrusion of a AA6082 aluminum alloy under different process conditions. Int J Adv Manuf Technol 129, 1585–1599 (2023). https://doi.org/10.1007/s00170-023-12397-8.
[45] (2024) fitrnet: Train neural network regression model. Mathworks. https://www.mathworks.com/help/stats/fitrnet.html Accessed 31 May 2024.
[46] Parson N, Fourmann J, Beland JF (2017) Aluminum Extrusions for Automotive Crash Applications. SAE Technical Papers. 1–16. https://doi.org/10.4271/2017-01-1272.

Appendix

Table 5: Final dataset used for training and testing ANN.

Exit temperature [°C]	Plastic strain	Maximum strain rate [s^{-1}]	Maximum Zener-Hollom parameter	Stored energy [J / mol*K]	Measured grain size [µm]	Training / test set allocation
485.4	4.8	25.9	2.61E+17	3.19E+05	105	TRAIN
534.5	6.6	7	7.50E+15	1.83E+05	115	TRAIN
530.6	5.9	20.2	2.56E+16	2.43E+05	107	TRAIN
529.9	5.3	4.5	5.88E+15	1.69E+05	128	TRAIN
532.2	6.2	16.6	1.96E+16	2.29E+05	133	TRAIN
526.8	4.6	13.4	2.00E+16	2.26E+05	92	TRAIN
529.6	5.3	14.2	1.88E+16	2.25E+05	114	TRAIN
487.7	5.5	44.3	3.99E+17	3.70E+05	81	TRAIN
487.2	5	40.5	3.74E+17	3.61E+05	95	TRAIN
482.2	4	9.4	1.11E+17	2.32E+05	95	TRAIN
509.5	4.6	1.9	6.15E+15	1.46E+05	130	TRAIN
527.5	4.9	15.5	2.25E+16	2.33E+05	108	TEST
482.2	4	9.7	1.14E+17	2.35E+05	77	TRAIN
482.2	3.9	9.1	1.07E+17	2.30E+05	93	TRAIN
482.2	3.9	9.2	1.08E+17	2.31E+05	133	TRAIN
525.7	4.4	15.8	2.48E+16	2.36E+05	77	TRAIN
531	7.1	27	3.36E+16	2.59E+05	136	TEST
482.3	4.1	10.3	1.21E+17	2.39E+05	81	TRAIN
523.5	3.1	2.8	4.84E+15	1.55E+05	196	TRAIN
482.5	4.3	11.2	1.30E+17	2.46E+05	89	TRAIN
526.6	4.6	19.1	2.88E+16	2.46E+05	87	TRAIN
530.1	5.7	23.9	3.09E+16	2.53E+05	118	TRAIN
525.5	3.6	3.6	5.69E+15	1.64E+05	151	TRAIN
534.3	11.5	49.6	5.36E+16	2.91E+05	80	TRAIN
520.1	2.9	1.6	3.21E+15	1.35E+05	161	TRAIN
484.2	4.6	19.9	2.12E+17	2.96E+05	78	TEST
527.2	6.3	78.6	1.15E+17	3.41E+05	122	TRAIN

482.2	4.2	11.1	1.31E+17	2.45E+05	67	TRAIN
519.9	4.8	3.6	7.29E+15	1.69E+05	155	TRAIN
527.3	7.7	148.4	2.17E+17	3.94E+05	115	TRAIN
483.3	4.2	12.6	1.40E+17	2.56E+05	108	TRAIN
484.1	5	28.6	3.07E+17	3.29E+05	161	TRAIN
519.4	3.8	1.7	3.52E+15	1.38E+05	148	TRAIN
481.9	3.9	9	1.07E+17	2.29E+05	161	TRAIN
521.7	2.9	1.6	2.99E+15	1.34E+05	122	TEST
516.3	3.1	1.7	4.04E+15	1.39E+05	155	TRAIN
524.8	4.5	28.5	4.65E+16	2.74E+05	87	TRAIN
524.1	4.3	23.1	3.89E+16	2.62E+05	99	TEST
563.1	4.8	140.2	4.60E+16	2.93E+05	103	TEST
521.8	3.8	14.9	2.77E+16	2.39E+05	111	TRAIN
522.1	3.9	14.5	2.66E+16	2.37E+05	135	TEST
523	4.1	14.3	2.52E+16	2.35E+05	87	TRAIN
522.8	3.9	16.3	2.90E+16	2.43E+05	75	TEST
523.6	4	17.1	2.94E+16	2.44E+05	86	TRAIN
526	4.5	20.3	3.14E+16	2.51E+05	64	TEST
531.4	3.8	7.5	9.18E+15	1.90E+05	94	TRAIN
527.1	5	23.2	3.42E+16	2.57E+05	67	TRAIN
533.9	5.6	7	7.69E+15	1.84E+05	104	TRAIN
534	4.7	6.2	6.78E+15	1.78E+05	151	TEST
537	6.7	68.9	6.63E+16	3.07E+05	112	TRAIN
555.1	4.1	59.1	2.68E+16	2.58E+05	92	TEST
538.2	7.3	54.8	5.01E+16	2.89E+05	86	TRAIN
550.8	3.8	45	2.43E+16	2.51E+05	83	TRAIN
535	5.2	27	2.83E+16	2.52E+05	62	TRAIN
535.8	25.2	17.6	1.78E+16	2.26E+05	113	TRAIN
552.7	3.9	48.6	2.43E+16	2.52E+05	95	TRAIN
548.7	3.6	45.5	2.68E+16	2.56E+05	88	TRAIN
539.8	4.3	15.1	1.29E+16	2.12E+05	167	TRAIN
550.3	3.8	45.3	2.50E+16	2.52E+05	79	TEST
533.3	4.8	20.9	2.36E+16	2.40E+05	67	TRAIN
551.7	3.9	47.3	2.46E+16	2.52E+05	89	TRAIN
538.7	6.5	21.8	1.95E+16	2.33E+05	164	TRAIN
552.2	3.9	48.2	2.46E+16	2.52E+05	76	TRAIN
533.7	4.9	21.2	2.35E+16	2.40E+05	131	TEST
552.8	4	49.6	2.47E+16	2.53E+05	91	TRAIN
561.2	4.5	103.8	3.67E+16	2.79E+05	109	TEST
533.9	23	174.6	1.92E+17	3.88E+05	103	TRAIN
567.7	5.8	233.8	6.38E+16	3.16E+05	137	TRAIN
536	6	30.9	3.10E+16	2.58E+05	120	TRAIN
596.7	5.1	169.4	1.53E+16	2.34E+05	116	TRAIN

529.4	4.2	17.1	2.28E+16	2.35E+05	107	TRAIN
577.2	5.3	135.4	2.55E+16	2.60E+05	104	TRAIN
533.4	4.7	22.2	2.49E+16	2.43E+05	88	TRAIN
537.6	8	52.7	4.94E+16	2.88E+05	72	TRAIN
533.4	2.8	6.7	7.52E+15	1.82E+05	125	TRAIN
528.4	16.9	6.2	8.64E+15	1.85E+05	137	TRAIN
551.2	39.5	81.6	4.33E+16	2.86E+05	119	TRAIN
551.3	26.2	73.7	3.90E+16	2.79E+05	96	TRAIN
574.3	5	119.9	2.53E+16	2.59E+05	78	TRAIN
597	5.1	175.8	1.57E+16	2.35E+05	74	TRAIN
551.6	17.1	67.5	3.53E+16	2.73E+05	70	TRAIN
513.9	5.4	5.4	1.43E+16	1.93E+05	81	TRAIN
558.4	4.3	48.1	1.90E+16	2.40E+05	69	TRAIN
558.3	4.2	44.6	1.77E+16	2.36E+05	84	TRAIN
554.5	4	40.9	1.90E+16	2.39E+05	107	TRAIN
552.3	13.1	67	3.40E+16	2.71E+05	76	TRAIN
562.1	4.4	9.2	3.14E+15	1.59E+05	108	TRAIN
516.3	3.5	5.6	1.33E+16	1.92E+05	78	TRAIN
554	3.9	57.2	2.71E+16	2.58E+05	100	TRAIN
523.5	3.8	6.8	1.17E+16	1.95E+05	135	TEST
557.5	4.2	46.2	1.90E+16	2.39E+05	69	TEST
549.2	15.1	128.6	7.42E+16	3.22E+05	67	TRAIN
542.5	19.1	104.9	8.00E+16	3.24E+05	73	TRAIN
512.3	24.5	7.7	2.19E+16	2.13E+05	124	TRAIN
538.3	11.4	57.7	5.25E+16	2.92E+05	70	TRAIN
563.7	4.8	78.5	2.51E+16	2.57E+05	105	TRAIN
521	6.1	8.5	1.64E+16	2.09E+05	98	TRAIN
535	7.7	24.8	2.60E+16	2.47E+05	82	TRAIN
558.3	4.3	48.2	1.92E+16	2.40E+05	72	TRAIN
524.5	3.8	6.3	1.04E+16	1.90E+05	100	TRAIN
559.4	4.2	46.1	1.75E+16	2.36E+05	76	TRAIN
525.3	3.9	6.6	1.05E+16	1.91E+05	119	TEST
534.3	8.4	23.2	2.51E+16	2.44E+05	90	TEST
555.3	4	40.9	1.84E+16	2.37E+05	79	TRAIN
559.1	4.4	48	1.85E+16	2.39E+05	60	TRAIN
531	6	17.6	2.19E+16	2.34E+05	126	TRAIN
564.8	6	89.4	2.74E+16	2.62E+05	64	TRAIN
524.9	4.3	13	2.11E+16	2.27E+05	99	TRAIN
524.8	6.1	13	2.12E+16	2.27E+05	98	TRAIN
527.2	4.8	14.5	2.13E+16	2.29E+05	123	TRAIN
482.5	6.5	24.1	2.79E+17	3.13E+05	121	TEST
531.5	7.9	31.9	3.89E+16	2.68E+05	107	TRAIN
526.5	5.6	15.8	2.39E+16	2.35E+05	123	TRAIN

526.9	4.7	16.3	2.42E+16	2.36E+05	97	TRAIN
482.1	4.1	10.4	1.23E+17	2.40E+05	97	TRAIN
482.9	5.3	20.1	2.28E+17	2.96E+05	124	TEST
536.1	3.4	7.7	7.70E+15	1.85E+05	119	TRAIN
531.6	7.8	30.3	3.68E+16	2.65E+05	107	TRAIN
483	4.1	10.8	1.22E+17	2.44E+05	119	TRAIN
481.8	3.8	9.2	1.10E+17	2.30E+05	191	TEST
528.8	5.2	22.2	3.04E+16	2.51E+05	137	TRAIN
483.7	4.3	15.2	1.66E+17	2.72E+05	103	TRAIN
533.4	8.8	39.2	4.40E+16	2.78E+05	97	TRAIN
483.1	4.4	13.8	1.55E+17	2.64E+05	123	TRAIN
530.7	7.5	40.7	5.13E+16	2.86E+05	80	TRAIN
481.9	3.8	9.4	1.12E+17	2.32E+05	154	TRAIN
531.5	6.3	47.2	5.75E+16	2.94E+05	89	TEST
527.3	3.5	9.6	1.40E+16	2.07E+05	84	TRAIN
528.3	7	6.7	9.38E+15	1.89E+05	126	TRAIN
526.7	5.7	56.4	8.46E+16	3.17E+05	121	TEST
483.4	4.6	17.6	1.95E+17	2.85E+05	76	TRAIN
526.7	4.9	26.4	3.96E+16	2.66E+05	108	TEST
482.4	4.4	11.9	1.39E+17	2.51E+05	93	TEST
526.2	4.3	20.2	3.10E+16	2.50E+05	98	TRAIN
482.5	4.7	13.3	1.54E+17	2.60E+05	71	TEST
533.6	2.8	7.1	7.90E+15	1.85E+05	135	TRAIN
522.9	4	17.7	3.14E+16	2.47E+05	123	TEST
482.4	5.3	15.8	1.84E+17	2.75E+05	107	TRAIN
523	4.1	13.2	2.33E+16	2.30E+05	163	TRAIN
487.8	5.1	41.8	3.74E+17	3.64E+05	124	TRAIN
524	3.9	14.1	2.38E+16	2.33E+05	141	TEST
508.5	20.3	7.3	2.47E+16	2.13E+05	137	TRAIN
567.1	6.3	393.5	1.10E+17	3.56E+05	106	TRAIN
521.7	3.9	15	2.80E+16	2.39E+05	150	TRAIN
558.3	4.8	90.2	3.59E+16	2.76E+05	144	TRAIN
524.2	3.9	14.9	2.50E+16	2.35E+05	228	TRAIN
555.3	4.1	60.9	2.73E+16	2.59E+05	97	TRAIN
514.7	5.9	10.2	2.61E+16	2.26E+05	83	TRAIN
522	3.9	15.6	2.88E+16	2.41E+05	132	TRAIN
558.7	4.9	89.3	3.49E+16	2.75E+05	96	TRAIN
525.9	4	16.8	2.61E+16	2.40E+05	145	TRAIN
520.7	4.3	11.1	2.17E+16	2.24E+05	112	TRAIN
559.3	4.8	68	2.60E+16	2.58E+05	101	TRAIN
524	4.1	17.6	2.97E+16	2.45E+05	125	TEST
553	4	50.8	2.51E+16	2.54E+05	96	TRAIN
526.1	3.8	6	9.24E+15	1.86E+05	102	TRAIN

550.9	3.8	45.5	2.45E+16	2.51E+05	87	TRAIN
528.3	4.5	21.3	2.98E+16	2.50E+05	86	TRAIN
525.7	16.5	7	1.10E+16	1.94E+05	126	TRAIN
526.4	4.7	21.9	3.33E+16	2.55E+05	96	TRAIN
560.9	5.2	77.3	2.77E+16	2.62E+05	75	TRAIN
550.9	3.8	48.3	2.60E+16	2.55E+05	105	TRAIN
530.9	7.1	44.8	5.60E+16	2.92E+05	81	TRAIN
529.2	7.2	41.6	5.60E+16	2.90E+05	84	TRAIN
547.6	3.7	44.1	2.72E+16	2.56E+05	81	TRAIN
530.5	10.9	82.3	1.05E+17	3.36E+05	107	TRAIN
559.4	4.9	71.1	2.70E+16	2.60E+05	98	TRAIN
552.4	3.9	47.8	2.42E+16	2.51E+05	88	TRAIN
516.2	3.8	6.8	1.62E+16	2.03E+05	87	TRAIN
514	4.9	12.2	3.22E+16	2.38E+05	170	TRAIN
538.5	7.6	68.6	6.19E+16	3.04E+05	127	TEST
559.8	5.2	87.1	3.26E+16	2.71E+05	78	TRAIN
556.6	4.2	65.4	2.79E+16	2.61E+05	110	TEST
535.2	6.1	36	3.74E+16	2.69E+05	90	TEST
513.8	8.1	9.4	2.50E+16	2.23E+05	76	TRAIN
534.9	5.3	28.8	3.03E+16	2.56E+05	102	TEST
533.6	5.2	25	2.78E+16	2.50E+05	106	TRAIN
529.1	5.6	187.6	2.54E+17	4.09E+05	100	TRAIN
525.6	7.1	9.9	1.56E+16	2.11E+05	101	TRAIN
563.9	5.5	77	2.44E+16	2.55E+05	100	TRAIN
536.9	6.4	40.8	3.94E+16	2.73E+05	100	TRAIN
531.5	4.5	17.2	2.10E+16	2.32E+05	110	TRAIN
564.5	5.8	82.3	2.55E+16	2.58E+05	98	TRAIN
561.5	4.7	58.7	2.05E+16	2.45E+05	100	TRAIN
535.6	5.8	31.2	3.19E+16	2.59E+05	89	TRAIN
555.9	4.2	44.4	1.95E+16	2.40E+05	96	TEST
530.7	4.3	16.5	2.08E+16	2.31E+05	88	TRAIN
528.6	3.2	6	8.29E+15	1.83E+05	147	TRAIN
562.3	4.9	68.8	2.33E+16	2.52E+05	131	TRAIN
528.1	4	15.2	2.15E+16	2.31E+05	93	TRAIN
536	6.1	32.2	3.23E+16	2.60E+05	117	TRAIN
558.1	4.1	44.3	1.78E+16	2.36E+05	97	TRAIN
552.9	3.9	40.9	2.03E+16	2.42E+05	120	TRAIN
530.4	4.3	17.8	2.27E+16	2.36E+05	105	TRAIN
531.5	3.8	12	1.46E+16	2.13E+05	105	TRAIN
537.1	6.5	35	3.35E+16	2.63E+05	105	TRAIN
566	4.5	66.9	1.95E+16	2.43E+05	104	TRAIN
559.6	4.3	48.9	1.84E+16	2.39E+05	121	TRAIN
535.5	6	11.3	1.16E+16	2.04E+05	107	TRAIN

532.8	4.6	21.6	2.49E+16	2.43E+05	90	TEST
536.9	17	11.4	1.10E+16	2.03E+05	166	TRAIN
538.5	6.8	39.9	3.60E+16	2.68E+05	134	TRAIN
554.7	4	42.3	1.95E+16	2.40E+05	93	TRAIN
534.4	5.3	28.3	3.04E+16	2.56E+05	85	TEST
563.9	5.1	93.9	2.98E+16	2.67E+05	78	TRAIN
559.9	4.5	52.5	1.96E+16	2.42E+05	91	TRAIN
536.7	7.5	50.4	4.91E+16	2.87E+05	84	TRAIN
551.2	48.5	87.7	4.66E+16	2.91E+05	128	TRAIN
537.3	3	8	7.60E+15	1.85E+05	100	TEST
561.2	4.7	57.2	2.02E+16	2.44E+05	84	TRAIN
563	5.4	69.2	2.28E+16	2.51E+05	74	TRAIN
589	5.6	187.4	2.25E+16	2.54E+05	115	TRAIN
531.4	5.1	10.5	1.28E+16	2.06E+05	115	TRAIN
552	16.4	75.3	3.87E+16	2.79E+05	99	TRAIN
529.6	14.2	178.9	2.37E+17	4.03E+05	91	TEST
552.4	12.8	65.1	3.29E+16	2.69E+05	109	TRAIN
531.1	9.3	23.2	2.88E+16	2.50E+05	114	TRAIN
552.2	12.1	60.1	3.06E+16	2.65E+05	63	TRAIN
521.4	2.9	2.1	3.98E+15	1.45E+05	124	TRAIN
523.3	4.3	3.8	6.62E+15	1.68E+05	225	TRAIN
521	3.7	2.7	5.21E+15	1.55E+05	126	TRAIN
518.1	15	10.2	2.24E+16	2.22E+05	202	TRAIN
517	27.8	13.9	3.20E+16	2.42E+05	106	TRAIN
528.9	4	5.7	7.77E+15	1.80E+05	170	TEST
530.5	4.3	8.7	1.11E+16	1.98E+05	84	TRAIN
529.9	11.1	14.3	1.87E+16	2.25E+05	83	TRAIN
529.4	3.8	6.9	9.21E+15	1.89E+05	112	TRAIN
520.5	4.4	2.5	4.93E+15	1.53E+05	181	TRAIN
532.8	3.9	8.7	1.00E+16	1.95E+05	122	TRAIN
522.6	3.2	2.7	4.85E+15	1.54E+05	127	TEST
537.1	4.2	13.2	1.26E+16	2.10E+05	153	TRAIN
519.3	5.4	3.9	8.11E+15	1.73E+05	151	TEST
528.1	6.5	5.5	7.76E+15	1.80E+05	134	TRAIN
517.6	4.2	3.8	8.53E+15	1.73E+05	96	TEST
526.5	3.2	2.5	3.78E+15	1.48E+05	134	TRAIN
520.1	5.3	4.3	8.63E+15	1.76E+05	131	TRAIN
522.4	2.9	1.9	3.44E+15	1.40E+05	149	TRAIN
517.2	4.5	3.2	7.31E+15	1.65E+05	209	TRAIN
518.6	3	1.6	3.43E+15	1.36E+05	164	TRAIN
514.1	3.3	2.1	5.51E+15	1.49E+05	213	TRAIN
530.4	3.8	7.8	9.97E+15	1.93E+05	97	TRAIN
532.1	4.1	9.4	1.12E+16	2.00E+05	115	TRAIN

533.9	4.6	5.8	6.37E+15	1.76E+05	117	TRAIN
537.9	4	14.7	1.36E+16	2.14E+05	120	TEST
539.6	5	19.6	1.69E+16	2.26E+05	158	TRAIN
539.1	3.9	15	1.32E+16	2.13E+05	106	TRAIN
533.4	4.2	4.5	5.05E+15	1.65E+05	103	TRAIN
534	6	6.8	7.44E+15	1.82E+05	104	TRAIN
534.3	12.7	4.2	4.54E+15	1.62E+05	106	TRAIN
535	8.1	6.3	6.60E+15	1.78E+05	145	TRAIN
534.4	7.7	7.1	7.64E+15	1.84E+05	128	TRAIN
534	22.7	100.7	1.10E+17	3.43E+05	89	TRAIN
533.4	6.1	6.8	7.63E+15	1.83E+05	122	TRAIN
533	7	10.2	1.16E+16	2.03E+05	123	TRAIN
532.4	5.6	6.2	7.27E+15	1.80E+05	137	TRAIN
526.7	4	8.5	1.28E+16	2.02E+05	121	TEST
524.9	3.7	6.9	1.12E+16	1.94E+05	115	TEST
524.5	3.5	5.1	8.43E+15	1.80E+05	123	TEST
523.7	3.2	5.5	9.41E+15	1.84E+05	102	TRAIN
521	5.9	9	1.74E+16	2.12E+05	112	TRAIN
518.5	5.4	10.2	2.20E+16	2.22E+05	97	TRAIN
514.2	9.4	9.4	2.46E+16	2.22E+05	112	TRAIN
511.8	13.4	9.4	2.74E+16	2.25E+05	111	TRAIN
512.1	7.1	13.6	3.91E+16	2.47E+05	106	TRAIN
525.2	4.5	10.5	1.68E+16	2.15E+05	138	TRAIN
527.4	5.9	9.5	1.38E+16	2.07E+05	127	TEST
530.4	4.5	7	8.94E+15	1.88E+05	114	TRAIN
532.7	3.4	9	1.04E+16	1.97E+05	204	TRAIN
521.4	4.9	8.3	1.57E+16	2.07E+05	179	TRAIN
514.6	4.9	7.1	1.82E+16	2.06E+05	90	TRAIN
514.9	4	5.8	1.47E+16	1.95E+05	133	TRAIN
514.2	4.2	5.8	1.52E+16	1.96E+05	95	TRAIN
514	4.9	5.5	1.45E+16	1.94E+05	100	TEST
526.1	6.9	15.8	2.43E+16	2.36E+05	105	TRAIN
524.8	5.9	12.7	2.07E+16	2.26E+05	112	TRAIN
522.8	6.6	9.7	1.73E+16	2.14E+05	120	TRAIN
525.3	6.8	27.3	4.36E+16	2.70E+05	132	TEST
529.2	4.4	11.5	1.55E+16	2.14E+05	127	TRAIN
535.1	3.7	7.7	8.04E+15	1.87E+05	116	TRAIN
530.4	3.7	7.1	9.07E+15	1.89E+05	126	TRAIN
528.9	3.5	9.6	1.31E+16	2.05E+05	101	TEST
523.2	4.2	12.2	2.13E+16	2.26E+05	133	TRAIN
519.2	4.4	12.3	2.57E+16	2.32E+05	127	TRAIN
516.6	6.6	8.5	1.99E+16	2.14E+05	93	TRAIN
508.9	13.1	7.5	2.49E+16	2.15E+05	129	TRAIN

507.8	8.8	8.3	2.90E+16	2.21E+05	100	TEST
526.8	8.6	6.9	1.03E+16	1.92E+05	136	TEST
530.3	3.7	7.6	9.75E+15	1.92E+05	132	TEST
533.2	6.8	16.7	1.89E+16	2.28E+05	180	TRAIN
520.6	4.7	8.4	1.65E+16	2.09E+05	138	TEST
514.7	3.9	5.8	1.48E+16	1.96E+05	111	TEST
514.6	3.7	7.1	1.82E+16	2.06E+05	122	TEST
513.9	4	6.9	1.83E+16	2.06E+05	113	TRAIN
525.6	6.1	10.2	1.61E+16	2.13E+05	124	TRAIN
526.4	4	18.4	2.80E+16	2.44E+05	80	TRAIN
528.1	3.2	13.6	1.92E+16	2.24E+05	103	TRAIN
528.6	3.2	6.2	8.56E+15	1.85E+05	133	TRAIN
530.3	3.9	10.1	1.30E+16	2.06E+05	140	TRAIN
533.4	5	15.7	1.76E+16	2.24E+05	161	TRAIN
534.6	5.1	14.4	1.54E+16	2.18E+05	133	TRAIN
534.3	4	13.8	1.49E+16	2.16E+05	107	TRAIN
532.7	6	38.1	4.41E+16	2.77E+05	105	TRAIN
530.3	6.1	14.3	1.83E+16	2.24E+05	110	TEST
531.1	7.5	23.8	2.95E+16	2.51E+05	104	TRAIN
530.9	10.4	24.2	3.03E+16	2.53E+05	133	TRAIN
529.7	22	19.5	2.57E+16	2.42E+05	123	TEST
530.6	3.8	14.1	1.79E+16	2.23E+05	109	TRAIN
533.2	4.1	15.4	1.74E+16	2.23E+05	95	TRAIN
536	10.8	20.4	2.05E+16	2.34E+05	127	TEST
537.2	16.8	11.6	1.11E+16	2.03E+05	119	TRAIN
537.9	4.7	10.4	9.63E+15	1.97E+05	158	TRAIN
537.8	3	8.5	7.91E+15	1.88E+05	152	TRAIN
537.4	3.9	10.5	9.93E+15	1.98E+05	142	TRAIN
537.1	2.8	8	7.67E+15	1.86E+05	151	TRAIN
524.1	4.3	4.3	7.23E+15	1.73E+05	187	TEST
519	6.5	5.8	1.22E+16	1.92E+05	194	TRAIN
522	3.1	2.4	4.43E+15	1.50E+05	210	TEST
519.3	4.6	3	6.24E+15	1.61E+05	184	TRAIN
519.4	4.6	2.6	5.38E+15	1.55E+05	202	TRAIN
519.7	4.6	2.4	4.90E+15	1.51E+05	182	TRAIN
524.4	10.8	6.1	1.01E+16	1.89E+05	185	TEST
520	4.5	2.8	5.65E+15	1.58E+05	143	TEST
530.3	5.9	8.4	1.08E+16	1.97E+05	172	TRAIN
530.6	4.5	7.3	9.25E+15	1.90E+05	131	TRAIN
523.6	5.1	3.8	6.53E+15	1.68E+05	151	TRAIN
518.2	9.2	3.6	7.86E+15	1.70E+05	160	TRAIN
530.2	4	5.1	6.57E+15	1.74E+05	122	TRAIN
529.1	5.4	15.2	2.05E+16	2.29E+05	146	TRAIN

518.2	8.7	6	1.31E+16	1.94E+05	123	TEST